Geometry and Solvent Dependence of the Electronic Spectra of the Amide Group and Consequences for Peptide Circular Dichroism

Jiří Šebek,[†,‡] Zdeněk Kejík,[‡] and Petr Bouř*[,†]

Institute of Organic Chemistry and Biochemistry, Academy of Sciences of the Czech Republic, Flemingovo nám. 2, 166 10, and Department of Analytical Chemistry, Institute of Chemical Technology, Technická 5, 166 28, Prague 6, Czech Republic

Received: February 8, 2006

The influence of geometry variations and solvent environment of *N*-methylacetamide on its energies and absorption intensities was systematically analyzed with the aid of the time-dependent density functional theory (TD DFT). Selective and often complicated reactions of individual electronic levels on the perturbations were found important for the resultant spectral profile. For example, the $n-\pi^*$ band position varied by tens of nanometers due to the C═O bond length oscillations, while it was rather unaffected by surrounding water. On the contrary, $\pi-\pi^*$ type transition energies and intensities were broadly dispersed by the aqueous environment but exhibited a modest coordinate dependence. A simple electrostatic model used previously for absorption in the IR region (*J. Chem. Phys.* **2005**, *122*, 144501) explained these changes only partially. Additionally, electronic transfer between the solute and the solvent had to be considered for faithful modeling of the ultraviolet light absorption. The inclusion of the environment and dynamics in the modeling then provided more accurate positions, intensities, and realistic inhomogeneous widths of spectral lines. These factors were found important for absorption and circular dichroism spectra of larger peptides and proteins. This was demonstrated with a combined DFT/coupled oscillator model providing principal features observed in electronic circular dichroism spectra of standard peptide conformations.

Introduction

Ultraviolet (UV) absorption spectra of the amide group have long provided a tool for determining the average secondary structure of peptides and proteins, exploring the dependence of the electronic transition frequencies and intensities on peptide geometry.[1,2] Namely, measuring the electronic circular dichroism (ECD), the difference in absorption of the left and right circularly polarized light, became a standard approach to interpreting protein structure.[3−6] The lowest-energy transitions, interpreted conventionally as $n-\pi^*$ and $\pi-\pi^*$, are accessible most easily in the region of wavelengths 180−240 nm.[7] The $n-\pi^*$ transition involves the carbonyl electron lone pair and is locally asymmetric with respect to the amide plane, while $\pi-\pi^*$ is symmetric and more spread over the amide-group conjugated π-system. Lately, vacuum techniques became available allowing use of light of much lower wavelengths and thus access to electronic states of higher energies.[8] The ultraviolet optical techniques thus parallel IR experiments where the absorption (IR) spectra (particularly the signal of the amide I, mostly C═O stretch) depend on the secondary structure as well[9−11] and Raman spectra where the amide III vibration (N−H deformation plus the C−N stretch coupled to the C−H wag) is used as a conformational marker.[12,13] More recently, vibrational circular dichroism (VCD) and Raman optical activity (ROA) have developed as complementary secondary structure analysis tools.[14,15] Typically, the interpretation of the differential techniques (ECD, VCD, and ROA) is more dependent on band shape than frequency.

Because of the importance for peptide spectroscopy, the electronic structure of the amide group has been extensively studied in the past.[1,2,16−21] The complex delocalized nature of the electronic phenomena and strong dynamic interactions with the solvent make reliable quantitative predictions quite difficult, namely, with respect to the limitations of computer power and theoretical apparatus. Recently, ab initio computations were made significantly easier by efficient implementations of the time-dependent density functional theory (TD DFT).[22−24] These enabled relatively reliable simulations of properties of the excited electronic states for fairly large molecules.[25] Other powerful tools consist of the combination of molecular dynamics and quantum mechanics (MD/QM) methods. Such partially empirical models provide qualitatively correct dependencies of spectral parameters on the temperature, molecular geometry, and solvent polarity.[19,20,26,27] However, simplified approaches are not universal. For example, the latest studies indicated that in aqueous environment water molecules actively participate in the amide transitions.[20,28] Thus, the popular dielectric continuum solvent model[29] may not be adequate for modeling electronic transitions or will have to be modified to capture the fast time response involved in the photon absorption.[19,30]

Yet, for practical applications, it is desirable not only to predict absorption frequencies but also to estimate accurately relative band intensities and inhomogeneous line widths and their dependence on the experimental conditions. Ideally, all factors including temperature, geometry variations, charge transfer, solvent polarity, and solute−solvent bonding should be taken into account. Therefore, as a part of the ongoing process of increasing the precision of the simulations, we attempt to quantitatively estimate the effect of the solvent and geometry variations on the amide-group electronic spectra. In this work,

* To whom correspondence should be addressed. E-mail: bour@uochb.cas.cz.
† Academy of Sciences.
‡ Institute of Chemical Technology.

10.1021/jp060813v CCC: $33.50
Published on Web 03/17/2006

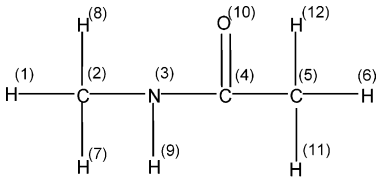

$\varphi = \angle(H^{(1)}\text{-}C^{(2)}\text{-}N^{(3)}\text{-}C^{(4)})$ 0 °
$\omega = \angle(C^{(2)}\text{-}N^{(3)}\text{-}C^{(4)}\text{-}C^{(5)})$ 180 °
$\psi = \angle(N^{(3)}\text{-}C^{(4)}\text{-}C^{(5)}\text{-}H^{(6)})$ 180 °

Figure 1. *N*-methylacetamide, atom numbering, and torsion angles pertaining to the reference conformation.

we also take advantage of our specific software that allows us to assign electronic transitions en masse, that is, to identify similar electronic states in a large number of molecules and thus automatically monitor changes in their energies and intensities under different circumstances.

The NMA molecule (Figure 1) in the trans-conformation was chosen in line with previous studies[31] as a convenient model of the amide group present in linear peptides that can be studied at a relatively high approximation level. To our surprise, we found striking differences in sensitivities of individual electronic transition energies and intensities to geometry changes and solvent perturbations. Some electronic states depend more on the geometry dispersion, some of them are more influenced by the participation of the water molecular orbital on the transition. A simple point charge approximation of the solvent used previously to model vibrational spectra[31−33] was found inadequate for the electronic transitions. Thus, a specific model is proposed for combined quantum/classical approaches so useful in predicting spectroscopic properties of the amide group.[34] Despite the complexity, some electronic properties of the amide group do appear transferable and, as shown below, suitable semiempirical schemes may yield not only realistic absorption profiles of NMA but also absorption and circular dichroism spectra of longer peptides and proteins.

Methods

The ab initio (DFT) computations were performed with the Gaussian program.[35] The time-dependent density functional theory[36] was used for computation of electronic excited states of NMA with the B3LYP functional[37] and Pople-type[38] (6-31G*, 6-31+G**, 6-311++G**) and Dunning's augmented correlation-consistent[39] (aug-cc-pVNZ, N = T, Q) basis sets as implemented in Gaussian. For comparison, results computed with the BHLYP half−half functional[40] are also reported; this and other trial DFT methods, however, always provided excitation energies and intensities inferior to the B3LYP values. Optimized geometry and corresponding vacuum transition parameters obtained at the B3LYP/6-311++G** level were used as a reference to which other computational approaches were compared. The COSMO[41,42] continuum solvent model was applied with the vacuum-optimized NMA geometry. Control computation with fully COSMO-optimized geometry leads to changes in wavelengths smaller than 2 nm. Within the harmonic approximation,[43] the sum of nuclear charge densities (density of nucleus J dependent on position $\mathbf{R}_J$ was obtained as $n(\mathbf{R}_J) = Z_J \int |f|^2 \Pi_{K\neq J} \mathrm{d}\mathbf{R}_K$, Z_J is the nuclear charge and f the vibrational wave function) was calculated with the B3LYP/6-311++G** force field.

For a realistic generation of water positions in clusters with NMA, a molecular dynamics (MD) simulation within the Tinker molecular dynamics package was explored.[44] The Amber94 force field[45] was used for a simulation of an NpT ensemble consisting of one NMA molecule in a cubic water cage (13.25 Å per side, $p = 1$ atm, $T = 298$ K). The MCM program[46] and our adjacent software were used for file manipulations and selections of first hydration water shells. Typically, hydrogen-bonded molecules within 3.6 Å from the closest NMA atom were retained as described below.

For comparison with previous works on solvent-induced vibrational frequency shifts[31,33,47,48] and to estimate the pure electrostatic influence of the solvent, we applied an empirical correction to energies of the NMA electronic transitions in water clusters. The transition wavelengths (λ) were obtained from their vacuum values (λ_0) as $\lambda = \lambda_0 + \sum_{i=1}^{4} b_i\varphi_i$, where φ_i is the solvent electrostatic field at the NMA atoms (i = H, N, C, O). The coefficients b_i were obtained from a fit to ab initio values, and the potentials were calculated approximating the water molecules by the Tinker atomic point charges (−0.84 for O, 0.42 for H).

Computed electronic transitions of NMA in the solvent or with geometry and basis set modifications were assigned automatically to those in the reference (B3LYP/6-311++G**/vac) system. The 10 lowest-energy transitions most relevant to the experimentally accessible region of wavelengths were considered. For the assignments, the reference geometry was rotated to achieve the best overlap (minimal root-mean-square (rms) atomic distances).[49] In the next step, the same rotation matrix was used for the rotation of p and d atomic orbitals. While the s-orbitals did not have to be rotated since they are not directional, the rotation of the f-orbitals not significantly participating in the lowest-energy states was neglected. This did not affect correct assignments, as was confirmed by visual inspection of the orbital shapes. Finally, overlaps $S_{IJ} = |\langle\bar{\Psi}_I|\Psi_J\rangle|$ between the $\bar{\Psi}_I$ and Ψ_J molecular orbitals of the reference and modified NMA molecules were calculated so that corresponding transitions could be identified on the basis of maximal overlap. Note, that absolute overlap values had to be compared because the phase of the wave function is immaterial.[50]

The last technical task consisted of generating peptide absorption and circular dichroism spectra from the NMA parameters. The transitional dipoles obtained ab initio were transferred to model polypeptides, Me-(L-Ala)$_{18}$-Me (for α-helix and random coil modeling) and (Me-(L-Ala)$_{19}$-Me)$_2$ (for β-sheet). One hundred independent configurations of each peptide and surrounding water molecules were generated during an MD run with the Tinker software (Amber94 force field, periodic solvent box, pressure of 1 atm, temperature of 298 K) so that the geometry dispersion could be modeled. The boxes with hydrated peptides are displayed in the Supporting Information. Standard peptide geometries[51] were used for initial conformations; the peptide geometries did not vary significantly during the simulation. The random coil was modeled with polyproline-like conformation, as experimental data suggest that at least locally the coil adopts this left-handed helical form.[52,53] The source amide-group transition energies and electric dipole moments were obtained from a vacuum calculation as well as from the average of the set of 90 NMA/water/COSMO clusters. During the transfer to the peptide, instantaneous geometry corrections were applied to amide transitions i according to the linear formula $\lambda_i = (1 + \sum_{j=1}^{N} p_{ij}(d_j - d_{j0}))\lambda_{i,0}$, where λ_i is the wavelength in the peptide and while λ_{i0} is the NMA value. For the coordinates (d_j, equilibrium values d_{j0}), the C═O, C(O)−N, and N−H bond lengths were considered ($N = 3$) and the coefficients p_{ij} were obtained from a fit of ab initio computations on NMA. Finally, the generalized transition dipole coupling approximation (TDC)[54,55] was used for estimation of the

TABLE 1: Calculated Energies (eV) of the 10 Lowest-Energy Transitions in NMA

transition	BHLYP 6-311++G**	B3LYP 6-31G**	B3LYP 6-31+G**	B3LYP 6-311++G**	B3LYP[a] 6-311++G**	B3LYP aug-cc-pVTZ	B3LYP aug-cc-pVQZ	MRCI[18] 6-31+G**	CASPT2[56] ANO/VTZ	exp[56]
1A″	6.08	5.75	5.78	5.71	5.61	5.69	5.69	5.56	5.49	5.5
2A″	6.39	7.50	5.95	5.73	5.71	5.71	5.71	6.14	5.96	
3A′	7.05	7.68	6.04	5.79	5.74	5.74	5.74	6.16	6.22	6.3
4A′	7.59	8.98	6.81	6.50	6.46	6.42	6.41	6.53	6.76	6.8
5A″	7.40	9.04	6.83	6.53	6.52	6.46	6.45	6.64	7.02	
6A′	7.84	9.37	7.09	6.77	6.67	6.63	6.62	6.89	6.93	
7A″	7.64	9.43	7.15	6.83	6.75	6.72	6.71	6.77	7.11	
8A′	7.93	7.38	7.25	7.04	6.86	6.81	6.79	7.46	7.03	7.1
9A″	8.30	10.21	7.39	7.09	7.04	6.81	6.78	7.02	7.12	
10A′	7.98	10.40	7.47	7.10	7.32	7.00	6.98	7.04	7.74	7.7
δ[b]	0.74	2.04	0.19	0.33	0.32	0.41	0.42	0.32	0.00	

[a] Reference conformation in this work ($\varphi = 0°$, $\psi = 180°$), but for consistency with the MRCI reference, all the other computations in this table are with $\varphi = 180°$ and $\psi = 180°$. [b] rms deviation from the MRCI value.

TABLE 2: Calculated Dipole Strengths (debye^2) of the 10 Lowest-Energy Transitions in NMA

	BHLYP 6-311++G**	B3LYP 6-31G**	B3LYP 6-31+G**	B3LYP 6-311++G**	B3LYP aug-cc-pVTZ	B3LYP aug-cc-pVQZ	MRCI[18] 6-31+G**	CASPT2[56] ANO(VTZ)
1A″	0.026	0.026	0.027	0.031	0.026	0.028	0.067	0.047
2A″	0.004	0.018	0.001	0.001	0.003	0.001	0.002	0.221
3A′	0.508	2.959	0.629	0.554	0.526	0.519	0.068	0.594
4A′	7.022	0.037	0.204	0.574	0.522	0.505	0.472	10.883
5A″	0.616	0.461	0.424	0.382	0.356	0.343	0.072	0.262
6A′	0.823	1.209	1.357	0.557	0.438	0.408	0.065	0.723
7A″	0.110	0.239	0.365	0.282	0.260	0.252	0.007	0.000
8A′	0.974	4.336	4.281	3.346	0.802	0.742	0.658	0.225
9A″	0.019	0.020	0.004	0.003	0.003	0.003	0.000	0.074
10A′	0.360	0.199	2.023	2.676	4.289	4.064	0.067	0.420

interaction of the electric dipole moments among peptide amide groups, so that the peptide absorption and circular dichroism spectra could be generated.

Results and Discussion

NMA Electronic Transitions. To estimate possible errors of the DFT method, 10 lowest electronic transition energies of NMA in a vacuum were calculated at multiple levels and compared with available benchmark MRCI and CASPT computations and experimental values[18,56] (Table 1). The MRCI/CASPT geometries differ in rotation of the methyl groups which, according to the control calculation (compare the fifth and sixth columns of the table), has apparently a minor effect on the magnitude and ordering on the energies. This reflects the predominant localization of the participating orbitals on the amide-group atoms, observed also for other amide derivatives.[56] Consequently, in peptides, the amide-group electronic system may be thus considered relatively isolated from the backbone, which justifies simplified amide−amide through-space interaction models.[57] Similar to the amide groups, protein side chain chromophores appear not to be coupled directly with respect to their interaction with visible light.[58] For more accurate results, however, a charge-transfer correction should be applied.[59]

In comparison with the influence of the methyl groups, the functional and basis set effect is more pronounced. The BHLYP functional (first column in Table 1) provides rather mediocre energies, often in an incorrect order. For the B3LYP functional, the smallest 6-31G** basis provides correct qualitative ordering, but the accuracy of the energies sharply deteriorates for higher-energy transitions. Clearly, the addition of the diffuse functions ("+" in 6-31+G**, 6-311++G**) is crucial for accurate computations. On the other hand, further extensions of the basis toward the aug-cc-pVNZ (N = T, Q) sets bring minor changes in calculated energies, all smaller than 0.2 eV. The triple- and quadruple-ζ correlation-corrected sets themselves provide essentially the same energies differing less than 0.5% within the entire range. For reasons of computational economy, we thus consider the 6-311++G** values to be reliable enough and use this intermediate basis further. The DFT energy values agree reasonably well with the MRCI and CASPT2 results reported previously,[18,56] although the highest-energy transitions are reproduced in different order and their assignment is somewhat problematic because of the state mixing.

The dipole strengths (Table 2) are more dependent on the approximation than the energies. The DFT with the 6-311++G** basis provides reasonable agreement (within ∼10−20%) with the aug-cc-pVNZ values for transitions 1−7, while the 6-311++G** dipole strength for transition number 8 appears significantly overestimated. The DFT values often deviate significantly from the wave function results, as do the MRCI and CASPT2 methods from each other. Although we consider the MRCI computation to be more reliable than CASPT2 (possibly affected by random degeneracies), the former method is dependent on the choice of the reference configurations; clearly obtaining more accurate spectral intensities with available computational methods appears rather difficult.[18]

Conventionally, the transitions are classified according to dominant orbital contributions to the electronic wave functions,[1] and for the amide group, the assignment for transitions in Tables 1 and 2 can be found elsewhere.[18,56] The $n-\pi^*$ and $\pi-\pi^*$ transitions are believed to be most important for peptide ECD.[7] The former (number one in Tables 1 and 2) is associated with the electron transfer from the lone nonbonded oxygen orbital to the π-system and has rather weak electric dipole strength while accompanied by a considerable magnetic transition moment.[7] The latter $\pi-\pi^*$ band can be associated particularly with transition number 8 in Tables 1 and 2 and involves a symmetric electronic shift within the amide π-system accompanied with a large transition electric dipole moment.

Geometry Variations. It is not computationally feasible to consider all the vibrational and electronic degrees of freedom of NMA in solution. However, apart from the Born−

TABLE 3: Variation of NMA Geometric Parameters Estimated from a Molecular Dynamic Run with Explicit Water Molecules

parameter	average	standard deviation	maximum−minimum
d(N−H) (Å)	1.01	0.026	0.12
d(C═O) (Å)	1.23	0.018	0.13
d(N−C(O)) (Å)	1.34	0.019	0.11
∠ N−C═O (deg)	124	2.6	15
∠ C−N−C−C (deg)	180	9	66

Oppenheimer (BO) approximation, we can suppose that during the interaction with photons electrons move much faster than nuclei and that the geometry of the excited electronic states does not have time to change during the process.[60] Within this static "vertical" model, we can investigate the dependence of the electronic transition parameters on the NMA ground-state geometry. For this purpose, variations of key geometry parameters were estimated on the basis of MD simulation of NMA in the water box. For 1000 MD configurations separated by one hundred 1 fs steps average, standard and maximal deviations of the C═O, N−H, C−N bond lengths, N−C═O bond angle, and the C−N−C−C (ω) torsion angle are summarized in Table 3. Apparently, the standard bond deviations are relatively small, with a maximum of 2.6% for the N−H. This bond is relatively weak, polar, and most influenced by formation of the hydrogen bonds with the solvent. But the distributions of the geometry parameters are broad and a relatively large deviation from the equilibrium values are possible, within the range given at the last column of Table 3. The N−H bond, for example, changes within ∼12% of its equilibrium values. The angle ω opposed by a soft torsional potential varies within ±30° during the MD simulation; the bond angle (N−C═O) exhibited rather large maximal (7.5°) but reasonable mean (2.6°) deviations around its equilibrium value. These values are in agreement with analogous simulations based on different force fields.[61]

For an alternative estimate of the amplitudes of the nuclear motions, we calculated nuclear charge densities quantum mechanically at the harmonic approximation with the B3LYP/6-311++G** force field. In this way, lower limits of the geometry variations can be obtained, without the solvent and temperature motion. The rotational and translational degrees of freedom were not included as they do not influence intrinsic NMA coordinates and consequently the optical spectra. As documented by Figure 2, the zero-point vibrations themselves cause large dispersions of the nuclear positions, for bond lengths almost comparable with those obtained by the classical mechanic MD model. Apparently, a large part of the amide-group geometry fluctuations thus stems from the harmonic vibrational motion. The dispersion of hydrogen positions is noticeably bigger than that of heavy atoms.

Geometry Dependence of Transition Energies and Intensities. How is the geometry dispersion reflected by the electronic spectra? Starting from the B3LYP/6-311++G** NMA equilibrium geometry (Figure 1), we changed independently the C═O, C−N, N−H bond lengths, the O═C−N bond angle, and the ω torsion angles and calculated the transition parameters in a vacuum and with the COSMO solvent correction. Variations of the angles φ and ψ produced minor energy changes and are not analyzed in detail. The dependencies of the transition energies are summarized in Figure 3. Clearly, the first lowest-energy transition ($n-\pi^*$) energy exhibits a striking dependence on the C═O bond length, only somewhat moderated by the continuum solvent model. Note, that the volatility of the $n-\pi^*$ carboxyl transition has also been confirmed for acetone.[62]

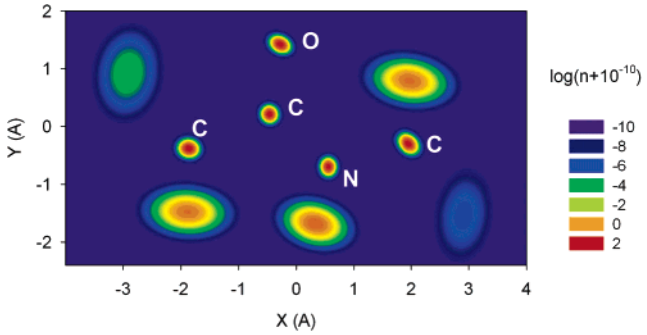

Figure 2. Total nuclear charge density (in the logarithmic scale) of NMA obtained at the harmonic approximation with the B3LYP/6-311++G** force field.

Obviously, in reality, the geometric changes cannot be separated from the influence of the environment.[61,62] But considering probable variations of the coordinates (Table 3, Figure 2), we can conclude that the transition can be dispersed within an interval of about 40 nm solely due to the geometry fluctuations! The energy of this transition also depends significantly on the C−N bond length, while, as expected, the influence of the remote N−H bond variation is negligible. Generally, the C═O bond length influence on the $\pi-\pi^*$ region transitions is rather modest, while these energies are notably influenced by the C−N bond length. Interestingly, the principal $\pi-\pi^*$ transition (number 8) behaves similarly as "satellite" transitions of similar symmetry and energy. Typically, variation of the C−N bond length within 0.1 Å, for example, can disperse the $\pi-\pi^*$ energy by ∼5 nm. The energy dependencies on the distance are fairly monotonic, except of the last scan over the angle ω. Changing the angle within 0···180° (although this is rather improbable in reality, cf. Table 3) causes dramatic reorganizations in the amide-group electronic structure and leads to a huge red shift of the absorption threshold for the transitional ($\omega = 90°$) geometry, by about 120 nm. Similar broadening of electronic (luminescence) spectra by torsional motion was found lately also for biphenyl.[63] Interestingly, electronic absorption energies of the planar *cis*- and *trans*-NMA conformers are quite similar. For the ω-scan, the orbital assignment was performed by comparison between neighboring geometries rather than by comparing to the equilibrium geometry. Note, however, that for all the scans the assignment of corresponding transitions is based on a rather unphysical concept of orbital similarity and may not be unambiguous. It helps, however, to explain and trace origins of observable dispersions of the absorption bands.

Transition dipole moments were found less dependent on the geometry variations. This reflects the fact that the dipoles are to a great extent determined by relatively stable shapes of molecular orbitals. For example, by varying the C═O bond length by ∼5%, one can expect similar relative change in the dipole strength as the dipole operator is proportional to the electron positions. As can be seen in Figure 4 for the dependence on the C═O bond length in a vacuum, however, occasional resonance of orbital energy levels and consequent orbital mixing may cause more profound changes (transitions 8 and 10).

Role of the Solvent. An aqueous environment can influence the electronic transitions by many mechanisms.[20,64] In the ground state, solvent molecules orient around polar solute groups, which creates an average solvent electrostatic field influencing the geometry, vibrational frequencies, and intensities.[31,32,48,65] However, charge transfer and interaction with water orbitals[66,67] cannot be neglected for studying of the excited electronic states. To compare the influence of these factors on the electronic

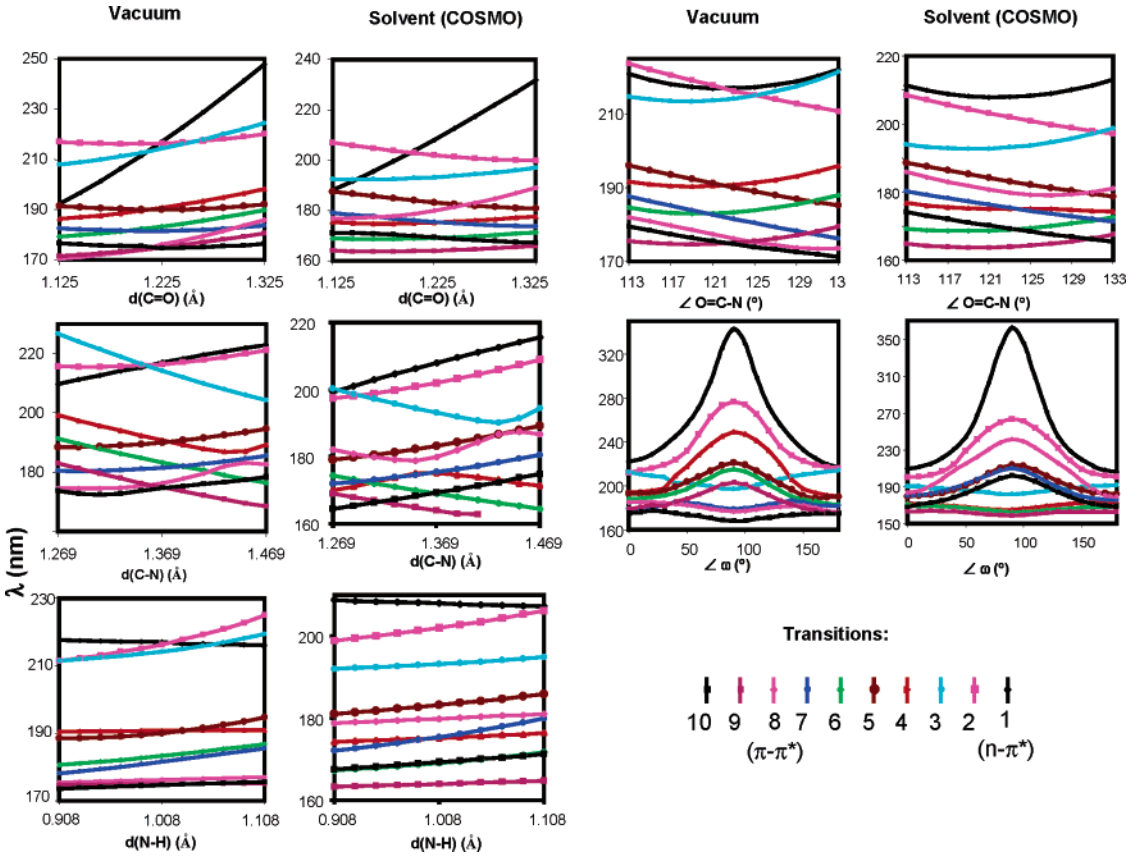

Figure 3. Calculated (B3LYP/6-311++G**) wavelength dependence of 10 lowest-energy electronic transitions in NMA on selected geometry parameters, in a vacuum and aqueous solvent (COSMO continuum).

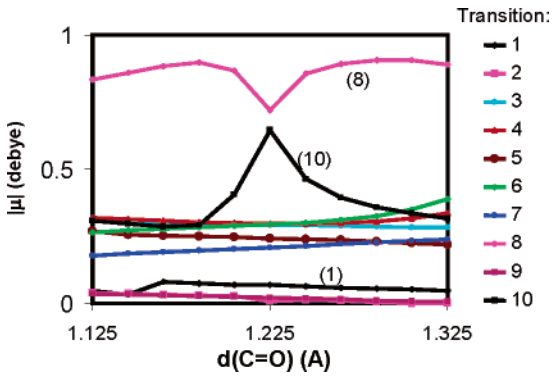

Figure 4. Calculated (TD DFT B3LYP/6-311++G**) dependence of the electric transition dipole moments on the C═O bond length.

spectra, energies and dipole strengths for NMA were calculated at the B3LYP/6-311++G** level in a vacuum, using the COSMO continuum solvent model and compared to values obtained as an average over a set of 90 clusters of NMA and 3−4 explicit hydrogen-bonded water molecules generated during the MD simulations. As follows from the summary of the results in Table 4, the solvent included via the COSMO model causes significant changes in energies and intensities, which indicates an important, although not dominant, role of the electrostatic interactions in the formation of the spectra. The changes for $\epsilon_r > 10$ (see the Supporting Information for details) are almost independent of the solvent relative permittivity. This is in agreement with the dielectric effect modeled by the Onsager function $((\epsilon - 1)/\epsilon)$,[68] quickly approaching unity for polar media. The almost homogeneous lowering of all wavelengths would cause an overall red shift of the absorption spectra, in favor of the agreement with the experiment for NMA.[69]

TABLE 4: Calculated (TDDFT/Becke3LYP/6-311++G) Wavelengths (λ) and Dipole Strengths (D) in NMA for Vacuum, COSMO, and Water Cluster Average**

	λ (nm)			D (debye^2)			
	vacuum	COSMO	clusters[a]	vacuum	COSMO	clusters[a]	R^b
1A″	217	208	208 (12)	0.03	0.03	0.09 (0.16)	0.97
2A″	216	202	244 (23)	0.00	0.07	0.05 (0.04)	0.18
3A′	214	193	229 (19)	0.55	0.90	0.11 (0.09)	0.54
4A′	191	175	183 (8)	0.57	1.31	1.37 (1.61)	0.78
5A″	190	183	187 (9)	0.38	0.30	0.86 (1.07)	0.79
6A′	183	169	184 (8)	0.56	0.33	0.78 (0.91)	0.54
7A″	182	175	189 (8)	0.28	0.43	0.87 (0.90)	0.52
8A′	176	180	182 (9)	3.35	9.10	2.29 (0.87)	0.87
9A″	175	164	188 (17)	0.00	0.01	0.27 (0.24)	0.32
10A′	175	169	182 (13)	2.68	1.82	1.96 (1.84)	0.49

[a] rms deviations for 90 clusters are given parentheses. [b] Correlation between the wavelengths obtained with the electrostatic and ab initio solvent models.

Contrary to the purely dielectric solvent influence modeled by COSMO, energy and intensity changes computed for the explicit NMA/water clusters (4./7. columns in Table 4, Figure 5) are bigger, with large positive and negative shifts, and, most importantly, do not correlate with the values obtained by the former model. For transition number 2, for example, the average cluster wavelength increases by 28 nm in comparison with a vacuum, while the COSMO model predicts a decrease of 14 nm. For individual clusters (Figure 5), even larger deviations than for the average values listed in Table 4 are possible. The lowest wavelengths are changed most by the interaction with water (transition number 2 changes within the interval 200−300 nm), while the dipoles change significantly within the entire range of transitions. The huge oscillations of the dipole strengths

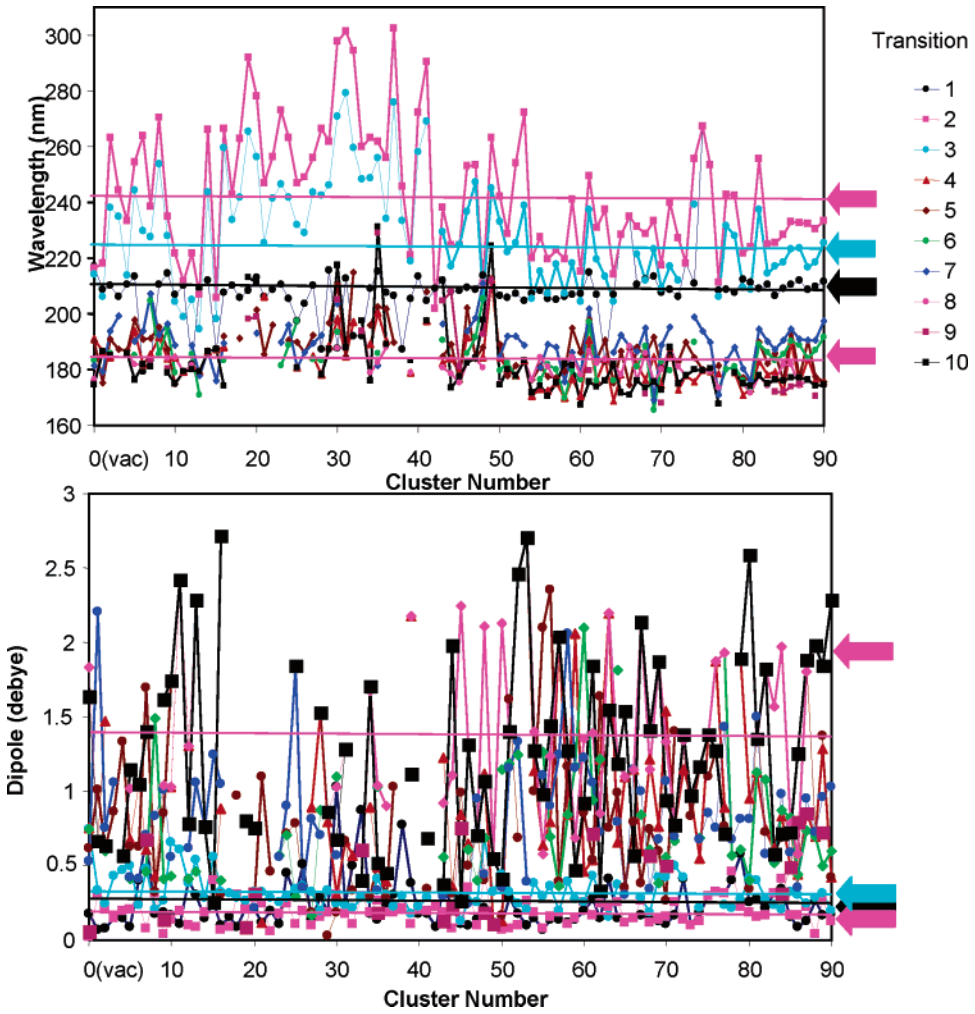

Figure 5. Calculated transition wavelengths (top) and dipole lengths (bottom) in 90 randomly selected clusters of NMA and 2−7 H-bonded water molecules. For transitions numbers 1, 2, 3, and 8, the NMA vacuum values (involved also as the cluster number 0) are indicated by the arrows at the right-hand side of the graphs. Connecting lines were added for easier orientation.

are also apparent from the root-mean-square deviations (Table 4) mostly comparable with or even bigger than the absolute values themselves. Additionally, the direction of the transition dipole vectors is significantly influenced by the hydrogen bonding. This is documented in Figure 6, where the $\pi-\pi^*$ transition moments in all the 90 clusters are overlapped. Although the dipole still oscillates around an average direction, the deviations are quite large and even significantly deviate from the molecular plane (cf. side view at the right-hand side of Figure 6). Detailed dipole changes for all transitions in clusters with the continuum solvent correction are given in the Supporting Information.

The way in which the explicit solvent participates on NMA electronic transitions can be illustrated for the strongest $\pi-\pi^*$ transition in Figure 7, where the main participating orbitals are plotted for NMA in a vacuum and for one randomly chosen NMA/H_2O cluster. In this case, the vacuum ground-state π orbital is perturbed by a water molecule H-bonded to the carbonyl oxygen. The excited π^* orbital is, at least visually, perturbed much less. We can thus interpret the solvent role in terms of pumping of solvent electrons into the solute excited orbitals during the light absorption. For other clusters and transitions cases when electrons are ejected into the solvent (= participation of solvent orbitals in NMA excited states) were observed. Such sharing of the solute and solvent orbital space during the amide-group excitations profoundly changes the

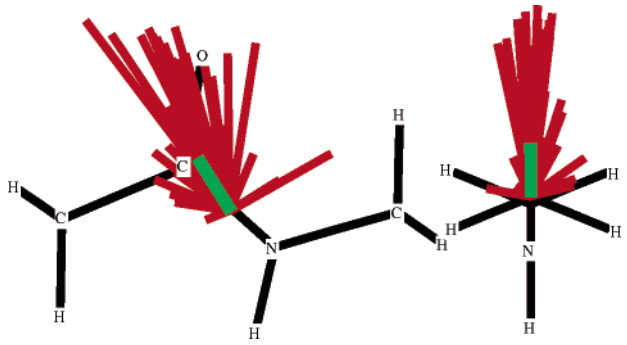

Figure 6. Transition dipole vectors (indicated by the red lines) for the transition number 8 ($\pi-\pi^*$) as obtained for the 90 water/NMA clusters. The vacuum dipole is indicated by the green line; parallel (left) and perpendicular (right) projections with respect to the molecular plane are plotted.

chromophore properties. Note, however, that relatively serious deficiencies of current DFT functionals used for the description of charge-transfer states were reported,[70,71] and thus, better theoretical models may be needed for more a accurate description of the solvent−solute interaction.

Point Charge Model. Unlike the COSMO continuum model, the point charge electrostatic correction (see the Methods) is sensitive to water positions and provides thus an alternative insight into the role of the electrostatic solvent influence on

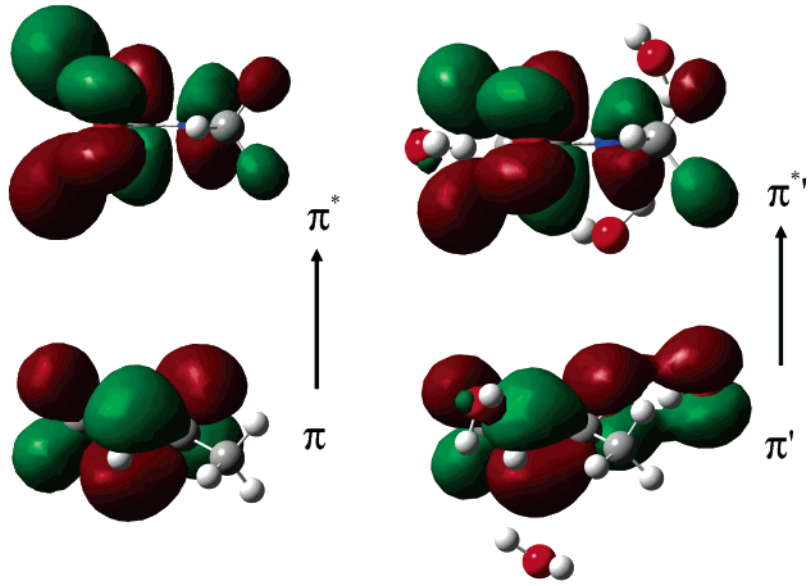

Figure 7. Example of principal orbitals participating at a $\pi-\pi^*$ transition of NMA in a vacuum (left) and at the corresponding transition in a cluster with three water molecules (right). In the cluster, the orbital π' is shared by NMA and one of the waters, while the excited orbital ($\pi^{*\prime}$, π^*) is approximately conserved in a vacuum and in the solvent.

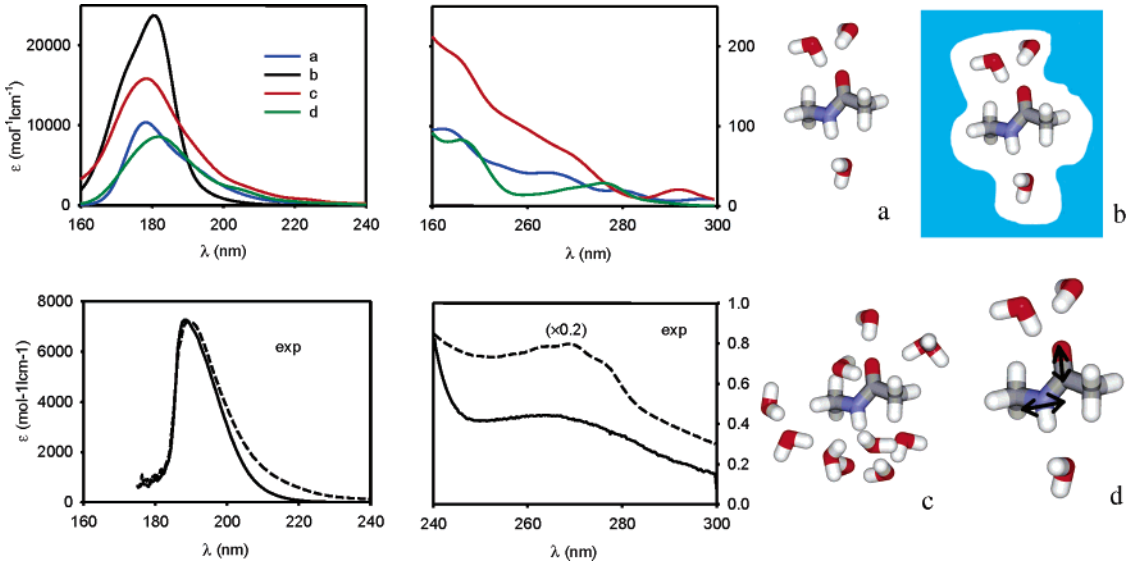

Figure 8. Averaged absorption spectra (a−d) calculated for four sets of NMA/water clusters schematically indicated at the right-hand side. Fixed (a) and unrestrained (d) NMA geometries and H-bonded water molecules, with additional COSMO continuum (b) and explicit (c) solvent models were used. The experimental NMA spectra (solid line, exp) at the lower part were obtained for 20 mg/L (within 160−240 nm) and 1 g/L (within 240−300 nm) aqueous solutions and 1 cm optical path length. As the dashed line, polyglycine spectra (for nearly saturated solutions) are inserted in the same figure and normalized to the maximal NMA absorption.

NMA transition energy shifts. For a subset of 11 NMA and water clusters, we compared ab initio (TD DFT B3LYP/6-311++G**) wavelengths with those ones obtained from the empirical correction. The correlation coefficients (R, listed in the last column of Table 4), however, indicate a very poor fitting, which is in a sharp contrast to the performance of the analogous model for vibrational frequencies, where the correlation with the ab initio results was nearly perfect.[31,33,48] Nevertheless, for several bands (namely, 1A″, 8A′), the coefficients do approach unity, which may indicate that for the transitions the electron transfer in the solvent is limited and that the electrostatic influence dominates. In fact, this can be independently confirmed also by the COSMO model, predicting wavelengths close to the average cluster values for these bands. On the other hand, the low correlation coefficient for the second transition, for example, suggests that the role of the electrostatics is minor in its overall shift. In this case, the continuum model also fails, providing wavelength changes in the opposite direction from the vacuum value than the explicit cluster model.

Absorption Profile. The role of various factors contributing to the UV absorption of NMA can be followed in Figure 8, where average spectra of four sets of 90 NMA/H_2O clusters are simulated and compared to experiment. To partially smooth the cluster intensities, Gaussian peaks 5 nm wide ($\exp(-(\Delta\lambda/5)^2)$) were applied. Relatively few spectral features can be compared. However, the absorption maximum in the $\pi-\pi^*$ region (experimentally at 186 nm) is reproduced only by ∼5 nm lower by the computations. The inhomogeneous line width and, namely, the absorption band slope in 200−240 nm appear relatively underestimated with the COSMO model (b), while the explicit computations (a, c, and d) overestimate the relative absorption in this region. The inclusion of the non-hydrogen-

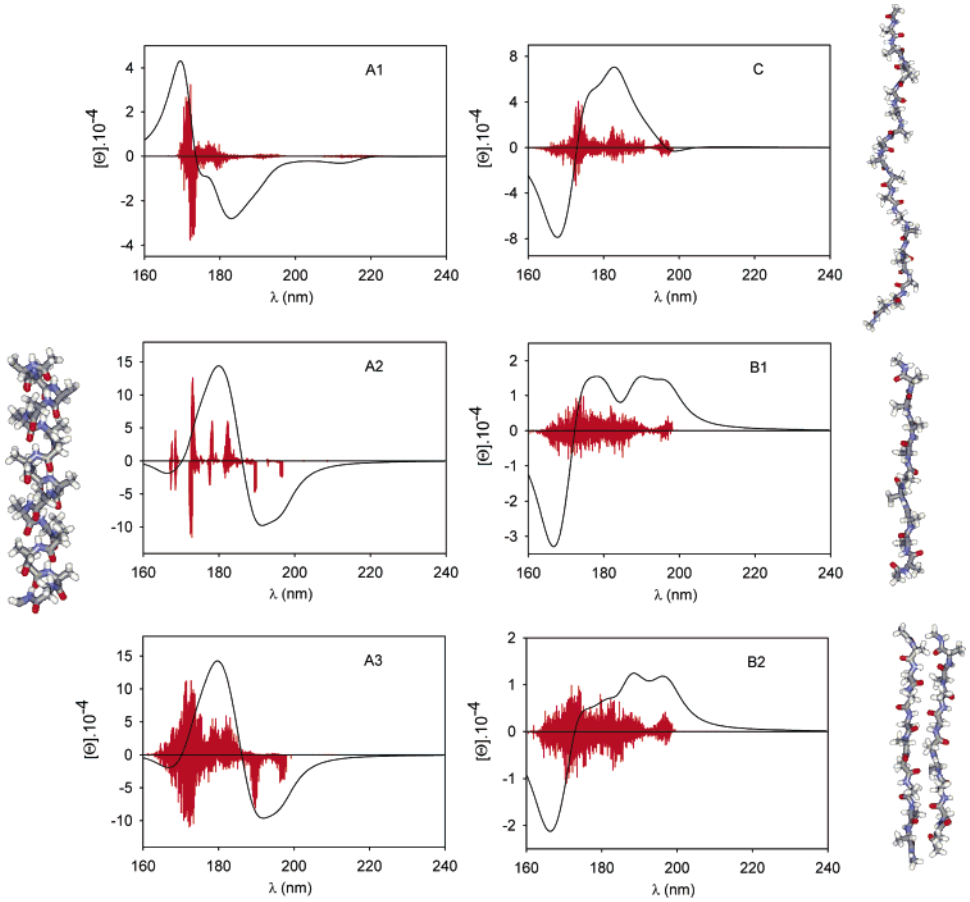

Figure 9. ECD spectra ([Θ] in deg cm^2 dmol^{-1}) of standard peptide secondary structures (A1−3 ... α-helix, C ... coil, and B1 and B2 ... one- and two-strand antiparallel β-sheet) simulated with the combined ab initio/TDC model. Vacuum (A1) and averaged NMA/water cluster/COSMO NMA amide-group parameters (A2−3, C, and B1−2) were used. The spectra were simulated without (A1 and A2) and with (A3, C, and B1−2) the correction on instantaneous peptide geometry.

bonded water molecules, either as the continuum (b) or explicitly (c), leads to a red shift and intensity increase of the absorption maximum. The absolute intensity (ϵ) is reproduced only approximately, which can be attributed to the complexity of the proper theoretical description of the polar interactions and is usual for these types of computation.[33,72] For completeness, we plot also the weak absorption in the 240−300 nm region in Figure 8, although the origin of this signal remains rather speculative. Most probably, solvent absorption would have to be consistently included for its interpretation.[66] This is also indicated by the different asymptotic behavior of the dielectric model (b) in comparison with the explicit model (c). The sharp drop of the experimental signal at ∼180 nm may be partially caused by spectrometer limits. The polyglycine experimental spectrum (dotted line) documents that the amide-group chromophore exhibits a relatively conservative absorption pattern in $(Gly)_n$ and NMA and that the NMA molecule is thus a good first-order approximation for models of peptide absorption of UV light.[2] However, fine differences in the two spectra can be found, namely, the red shift of the absorption maximum of $(Gly)_n$ (188 → 189.3 nm) and increased intensity of the shoulder at ∼215 nm. The experimental spectra are consistent with literature data for amides.[69]

Peptide ECD Spectra. While the absorption spectra of *N*-methylacetamide are currently of little practical interest, peptide and protein ultraviolet (electronic) circular dichroism has been established as a useful analytical method in biochemistry for a long time.[73] Thus, we would like to know the extent to which the ECD spectra of standard peptide secondary structures are influenced by the solvent and geometry dispersion. This can be estimated for simulated spectra of α-helix (A1−A3) at the left-hand side of Figure 9. The vacuum NMA transition energies and dipole moments (A1) provide quite an unrealistic spectral profile. On the other hand, energies and moments obtained from the averaging over the set of NMA/water clusters involving the COSMO continuum (A2) yield a CD spectrum that can be nicely related to typical experimental spectra of α-helical peptides and proteins.[73−76] (Examples of experimentally derived spectra of α-helices and other peptide secondary structures are given in the Supporting Information.) Although the spectral envelope does not change much when the correction onto instantaneous peptide MD geometry is included (trace A3), from the dispersion of the individual transitions included as the red lines, we can see that the geometry variations significantly contribute to the overall inhomogeneous broadening of spectral lines. On average, the calculated band positions are rather too low, but this is usual for the anticipated approximation[20,61,62,77] and should not influence the principal spectral shape given predominantly by special orientation of the amide chromophores.[78] Note, that no arbitrary scaling of the ab initio NMA frequencies was applied. The dominant maximum at 180 nm thus corresponds to the analogous experimental band at ∼190 nm of the same sign. Also, the minimum at 192 nm can be seen around 205 nm, as well as the famous "helical band" calculated as a negative shoulder at 196, experimentally at ∼220 nm.[74,79] Namely, this latter band could not be reproduced previously with vacuum ab initio models.[2] The absolute intensities ([Θ], molar elipticity) match within

~50% of the values reported experimentally, which again represents a very good agreement given the approximations involved. The experimental relative intensity of the helical band at 220 nm is somewhat bigger than predicted, which can be perhaps explained by the contribution of the peptide chain neglected in the model. Indeed, the absorption intensity of polyglycine is bigger than that for NMA in this region (Figure 8). Obviously, models where some parameters are empirically adjusted lead to better quantitative agreement with the experiment,[75,80] but we suppose that our parallel approach based strictly on ab initio results may become more universal. For example, using the same methodology, we could also reproduce all the main features of the unordered (often referred to as coil or random conformation[81]) secondary structures plotted as trace C in Figure 9. Particularly, the negative signal calculated at 169 nm is observed within 195−197 nm, so is the positive maximum at 183 nm (experimentally 208−212 nm) and the weak negative lobe at 199 nm (observed at 228 nm).[74,79,82] Retrospectively, the simulation also confirms previous propositions to assign the left-handed polyproline II-like peptide helix to this structure.[52,53,81]

For the one- and two-strand β-strands (traces B1−B2 in Figure 9), we did not find satisfactory agreement with available experimental data. Particularly, the positive signal calculated at ~190 nm is usually observed only for proteins with high turn content, while for pure sheets a negative signal is reported in this region.[74,79,82] Despite this, we believe that the simulations are still meaningful. First, there exists no standard β-sheet ECD spectra, and available data usually obtained as an abstraction from a series of measurements often differ according to their source.[83] Also, the signal for flat sheets is very small, which is in agreement with the simulations (note the *y*-scales). Finally, because of the nearly planar symmetry, principal contributions to the ECD signal of the sheets may come from the sheet twist, amino acid side chains, and different hydration patterns of the amide group in NMA and in the peptides,[84] factors all of which currently could not be included in the modeling. On the other hand, the noticeable difference between the spectral shapes of one- and two-strand sheets (B1 and B2) give us a hope that proper simulations in the future may provide a tool for extraction of finer structural details omitted in peptide ECD spectroscopy so far. Because of the long-range and environmental sensitivity of this type of spectroscopy it may, in this context, become at least a convenient complementary technique for studying β-sheet and β-fibril formations, including those in the prion-involving degenerative diseases.[85]

Conclusions

The combined quantum mechanics/molecular mechanics models represent powerful tools for simulations of optical properties of complex systems. For the absorption of ultraviolet light, special attention has to be paid to correct involvement of geometry and environmental variations determining energies and intensities of the electronic transitions. The polar amide group of *N*-methylacetamide interacts strongly with the aqueous solvent. Both a bulk electrostatic influence as well as a direct sharing of the orbitals involved in the light absorption between the solute and the solvent change the spectral parameters significantly. Water molecules directly hydrogen-bonded to the solute account for most of the changes. However, substitutions of the remaining solvent explicitly and by a continuum (traces b, c in Figure 8) did not produce entirely analogous effects, which we could not explain. For the geometric variations, zero-point vibrations already cause a broad dispersion of the spectral bands. Individual orbitals and electronic transitions exhibit very different susceptibilities to these factors. Despite this complexity, NMA and peptide absorption and ECD spectra could be reliably simulated in the spirit of the ab initio computations with a simplified model. Not being dependent on empirical parameters, this approach potentially allows one to extract more structural information from optical spectra of peptides and proteins. In the future, however, other factors, such as amino acid side chains, β-sheet twist and secondary structure irregularities, and different hydration patterns in hydrophobic and hydrophilic structural motifs will have to be accounted for.

Acknowledgment. This work was supported by the Grant Agency of the Czech Republic (Grant 203/06/0420) and an internal grant of the Institute of Chemical Technology (402080017).

Supporting Information Available: Detailed parameters of the dipole coupling model for simulations of the peptide ECD spectra, relative permittivity dependence of NMA transitions, and some examples of experimental spectra of peptides and proteins. This material is available free of charge via the Internet at http://pubs.acs.org.

References and Notes

(1) Besley, N. A.; Hirst, J. D. *J. Am. Chem. Soc.* **1999**, *121*, 936.
(2) Hirst, J. D.; Colella, K.; Gilbert, A. T. B. *J. Phys. Chem. B* **2003**, *107*, 11813.
(3) *Circular Dichroism Principles and Applications*; Berova, N., Nakanishi, K., Woody, R. W., Eds.; Wiley-VCH: New York, 2000.
(4) Sreerama, N.; Woody, R. W. Circular dichroism of peptides and proteins. In *Circular Dichroism Principles and Applications*; Nakanishi, K., Berova, N., Woody, R. W., Eds.; Wiley-VCH: New York, 2000; p 601.
(5) Venyaminov, S. Y.; Yang, J. T. Determination of Protein Secondary Structure. In *Circular Dichroism and the Conformational Analysis of Biomolecules*; Fasman, G. D., Ed.; Plenum Press: New York, 1996; p 69.
(6) Volosov, A.; Woody, R. W. Theortical approach to natural electronic optical activity. In *Circular Dichroism: Principles and Applications*; Nakanishi, K., Berova, N., Woody, R. W., Eds.; VCH Publishers: New York, 1994; p 59.
(7) *Circular Dichroism Principles and Applications*; Nakanishi, K.; Berova, N.; Woody, R. W., Eds.; VCH: New York, 1994.
(8) Matsuo, K.; Fukuyama, T.; Yonehara, R.; Namatame, H.; Taniguchi, M.; Gekko, K. *J. Electron. Spectrosc. Relat. Phenom.* **2005**, *144*, 1023.
(9) Mantsch, H. H.; Chapman, D. *Infrared Spectroscopy of Biomolecules*; Wiley-Liss: Chichester, U.K., 1996.
(10) Haris, P. I.; Chapman, D. *Biopolymers* **1995**, *37*, 251.
(11) Keiderling, T. A.; Silva, R. A. G. D. Conformational studies using infrared techniques. In *Synthesis of peptides and peptidomimetics*; Goodman, M. e. a., Ed.; Georg Thieme Verlag: Stuttgart, Germany, 2002; Vol. E22b.
(12) Williams, R. W. *Methods Enzymol.* **1986**, *130*, 311.
(13) Asher, S. A.; Ianoul, A.; Mix, G.; Boyden, M. N.; Karnoup, A.; Diem, M.; Schweitzer-Stenner, R. *J. Am. Chem. Soc.* **2001**, *123*, 11775.
(14) Barron, L. D.; Hecht, L. Vibrational Raman optical activity: From fundamentals to biochemical applications. In *Circular dichroism, principles and applications*, 2nd ed.; Nakanishi, K., Berova, N., Woody, R. W., Eds.; Wiley-VCH: New York, 2000; p 667.
(15) Baello, B.; Pančoška, P.; Keiderling, T. A. *Anal. Biochem.* **2000**, *280*, 46.
(16) Besley, N. A.; Brienne, M. J.; Hirst, J. D. *J. Phys. Chem. B* **2000**, *104*, 12371.
(17) Hirst, J. D. *J. Chem. Phys.* **1998**, *109*, 782.
(18) Hirst, J. D.; Hirst, D. M.; Brooks, C. L. *J. Phys. Chem. A* **1997**, *101*, 4821.
(19) Cammi, R.; Corni, S.; Mennucci, B.; Tomasi, J. *J. Chem. Phys.* **2005**, *122*, 104513.
(20) Mennucci, B.; Martinez, J. M. *J. Phys. Chem. B* **2005**, *109*, 9818.
(21) Jalkanen, K. J.; Elstner, M.; Suhai, S. *J. Mol. Struct. (THEOCHEM)* **2004**, *675*, 61.
(22) Stratmann, R. E.; Scuseria, G. E.; Frisch, M. J. *J. Chem. Phys.* **1998**, *109*, 8218.
(23) Pecul, M.; Ruud, K.; Helgaker, T. *Chem. Phys. Lett.* **2004**, *388*, 110.
(24) Furche, F.; Alhrichs, R. *J. Chem. Phys.* **2004**, *121*, 12772.

(25) Rogers, D. M.; Besley, N. A.; O'Shea, P.; Hirst, J. D. *J. Phys. Chem. B* **2005**, *109*, 23061.
(26) Besley, N. A.; Oakley, M. T.; Cowan, A. J.; Hirst, J. D. *J. Am. Chem. Soc.* **2004**, *126*, 13502.
(27) Besley, N. A. *Chem. Phys. Lett.* **2004**, *390*, 124.
(28) Rocha, W. R.; De Almeida, K. J.; Coutinho, K.; Canuto, S. *Chem. Phys. Lett.* **2001**, *345*, 171.
(29) Pecul, M.; Marchesan, D.; Ruud, K. *J. Chem. Phys.* **2005**, *122*, 024106.
(30) Caricato, M.; Ingrosso, F.; Mennucci, B.; Tomasi, J. *J. Chem. Phys.* **2005**, *122*, 154501.
(31) Bouř, P.; Michalík, D.; Kapitán, J. *J. Chem. Phys.* **2005**, *122*, 144501.
(32) Bouř, P. *J. Chem. Phys.* **2004**, *121*, 7545.
(33) Bouř, P.; Keiderling, T. A. *J. Chem. Phys.* **2003**, *119*, 11253.
(34) Yang, S.; Cho, M. *J. Chem. Phys.* **2005**, *123*, 134503.
(35) Frisch, M. J.; Trucks, G. W.; Schlegel, H. B.; Scuseria, G. E.; Robb, M. A.; Cheeseman, J. R.; Montgomery, J. A.; Vreven, J. T.; Kudin, K. N.; Burant, J. C.; Millam, J. M.; Iyengar, S. S.; Tomasi, J.; Barone, V.; Mennucci, B.; Cossi, M.; Scalmani, G.; Rega, N.; Petersson, G. A.; Nakatsuji, H.; Hada, M.; Ehara, M.; Toyota, K.; Fukuda, R.; Hasegawa, J.; Ishida, M.; Nakajima, T.; Honda, Y.; Kitao, O.; Nakai, H.; Klene, M.; Li, X.; Knox, J. E.; Hratchian, H. P.; Cross, J. B.; Adamo, C.; Jaramillo, J.; Gomperts, R.; Stratmann, R. E.; Yazyev, O.; Austin, A. J.; Cammi, R.; Pomelli, C.; Ochterski, J. W.; Ayala, P. Y.; Morokuma, K.; Voth, G. A.; Salvador, P.; Dannenberg, J. J.; Zakrzewski, V. G.; Dapprich, S.; Daniels, A. D.; Strain, M. C.; Farkas, O.; Malick, D. K.; Rabuck, A. D.; Raghavachari, K.; Foresman, J. B.; Ortiz, J. V.; Cui, Q.; Baboul, A. G.; Clifford, S.; Cioslowski, J.; Stefanov, B. B.; Liu, G.; Liashenko, A.; Piskorz, P.; Komaromi, I.; Martin, R. L.; Fox, D. J.; Keith, T.; Al-Laham, M. A.; Peng, C. Y.; Nanayakkara, A.; Challacombe, M.; Gill, P. M. W.; Johnson, B.; Chen, W.; Wong, M. W.; Gonzalez, C.; Pople, J. A. *Gaussian 03*; Gaussian, Inc.: Pittsburgh, PA, 2003.
(36) Furche, F.; Ahlrichs, R. *J. Chem. Phys.* **2002**, *116*, 7433.
(37) Becke, A. *Phys. Rev. A* **1988**, *38*, 3098−3100.
(38) Krishnan, R.; Binkley, J. S.; Seeger, R.; Pople, J. A. *J. Chem. Phys.* **1980**, *72*, 650.
(39) Davidson, E. R. *Chem. Phys. Lett.* **1996**, *260*, 514.
(40) Becke, A. D. *J. Chem. Phys.* **1993**, *98*, 1372.
(41) Klamt, A.; Schuurmann, G. *J. Chem. Soc., Perkin Trans.* **1993**, *2*, 799.
(42) Klamt, A. COSMO and COSMO-RS. In *The Encyclopedia of Computatinal Chemistry*; Schleyer, P. R., Allinger, N. L., Clark, T., Gasteiger, J., Kollman, P. A., Schaefer, H. F., III, Schreiner, P. R., Eds.; John Wiley & Sons: Chichester, U.K., 1998; Vol. 1; p 604.
(43) Papoušek, D.; Aliev, M. R. *Molecular Vibrational/Rotational Spectra*; Academia: Prague, Czech Republic, 1982.
(44) Ponder, J. W. *Tinker, Software Tools for Molecular Design*, 3.8 ed.; Washington University School of Medicine: Saint Louis, MO, 2000.
(45) Cornell, W. D.; Cieplak, P.; Bayly, C. I.; Gould, I. R.; Merz, K. M.; Ferguson, D. M.; Spellmeyer, D. C.; Fox, T.; Caldwell, J. W.; Kollman, P. A. *J. Am. Chem. Soc.* **1995**, *117*, 5179.
(46) Bouř, P.; Maloň, P. *MCM Molecular Graphics*; Academy of Sciences: Prague, Czech Republic, 1995−2005.
(47) Lee, H.; Kim, S. S.; Choi, J. H.; Cho, M. *J. Phys. Chem. B* **2005**, *109*, 5331.
(48) Choi, J. H.; Cho, M. *J. Chem. Phys.* **2004**, *120*, 4383.
(49) Bouč, P.; Sopková, J.; Bednárová, L.; Maloň, P.; Keiderling, T. A. *J. Comput. Chem.* **1997**, *18*, 646.
(50) Szabo, A.; Ostlund, N. S. Modern quantum chemistry. *Introduction to advanced electronic structure theory*; Dover: New York, 1989.
(51) Richardson, J. S.; Richardson, D. C. Principles and patterns of protein conformation. In *Prediction of Protein Structure and the Principles of Protein Conformation.*; Fasman, G. D., Ed.; Plenum: New York, 1989; p 1.
(52) Dukor, R. K.; Keiderling, T. A. *Biopolymers* **1991**, *31*, 1747.
(53) Woody, R. W. *Adv. Biophys. Chem.* **1992**, *2*, 37.
(54) Holzwarth, G.; Chabay, I. *J. Chem. Phys.* **1972**, *57*, 1632.
(55) Xiang, T.; Goss, D. J.; Diem, M. *Biophys. J.* **1993**, *65*, 1255.
(56) Serrano-Andres, L.; Fülscher, M. P. *J. Am. Chem. Soc.* **1997**, *118*, 112190.
(57) Rogers, D. M.; Hirst, D. M. *Chirality* **2004**, *16*, 234.
(58) Rogers, D. M.; Hirst, D. M. *Biochemistry* **2004**, *43*, 11092.
(59) Gilbert, A. T. B.; Hirst, J. D. *J. Mol. Struct. (THEOCHEM)* **2004**, *675*, 53.
(60) *The Encyclopedia of Computational Chemistry*; Schleyer, P. R., Allinger, N. L., Clark, T., Gasteiger, J., Kollman, P. A., Schaefer, H. F., III, Schreiner, P. R., Eds.; John Wiley & Sons: Chichester, U.K., 1998.
(61) Hayashi, T.; Zhuang, W.; Mukamel, S. *J. Am. Chem. Soc.* **2005**, *109*, 9747.
(62) Aidas, K.; Kongsted, J.; Osted, A.; Mikkelsen, K. V. *J. Phys. Chem. A* **2005**, *109*, 8001.
(63) Beenken, W. J. D.; Lischka, H. *J. Chem. Phys.* **2005**, *123*, 144311.
(64) Improta, R.; Barone, V. *J. Am. Chem. Soc.* **2004**, *126*, 14320.
(65) Florian, J.; Warshel, A. *J. Phys. Chem. B* **1997**, *101*, 5583.
(66) Prendergast, D.; Grossman, J. C.; Galli, G. *J. Chem. Phys.* **2005**, *123*, 014501.
(67) Chipman, D. M. *J. Chem. Phys.* **2005**, *122*, 044111.
(68) Onsager, L. *J. Am. Chem. Soc.* **1936**, *58*, 1486.
(69) Nielsen, E. B.; Schellman, J. A. *J. Phys. Chem.* **1967**, *71*, 2297.
(70) Dreuw, A.; Head-Gordon, M. *J. Am. Chem. Soc.* **2004**, *126*, 4007.
(71) Tozer, D. J. *J. Chem. Phys.* **2003**, *119*, 12697.
(72) Bouř, P. *Chem. Phys. Lett.* **2002**, *365*, 82.
(73) Fasman, G. D. *Circular Dichroism and the Conformational Analysis of Biomolecules*; Plenum: New York, 1996.
(74) Brahms, S.; Brahms, J. *J. Mol. Biol.* **1980**, *138*, 149.
(75) Chin, D. H.; Woody, R. W.; Rohl, C. A.; Baldwin, R. L. *Proc. Natl. Acad. Sci. U.S.A.* **2002**, *11*, 15416.
(76) Larack, S. A.; Martenson, R. E. *Biochemistry* **1985**, *24*, 6666.
(77) Bouř, P. *Chem. Phys. Lett.* **2001**, *345*, 331.
(78) Barron, L. D. *Molecular Light Scattering and Optical Activity*; Cambridge University Press: Cambridge, U.K., 2004.
(79) Johnson, W. C. *Proteins* **1999**, *35*, 307.
(80) Clark, L. B. *J. Am. Chem. Soc.* **1995**, *117*, 7974.
(81) Dukor, R. K.; Keiderling, T. A. *Biospectroscopy* **1996**, *2*, 83.
(82) Greenfield, N.; Fasman, G. D. *Biochemistry* **1969**, *8*, 4108.
(83) Keiderling, T. A.; Wang, B.; Urbanová, M.; Pančoška, P.; Dukor, R. K. *Faraday Discuss.* **1994**, *99*, 263.
(84) Bouř, P.; Keiderling, T. A. *J. Phys. Chem. B* **2005**, *109*, 23687.
(85) Dupiereux, I.; Zorzi, W.; Lins, L.; Brasseur, R.; Colson, P.; Heinen, E.; Elmoualij, B. *Biochem. Biophys. Res. Commun.* **2005**, *331*, 894.